Thin Solid Films, *250* (1994) 92–100

Electronic and crystallographic structure of γ-alumina thin films

B. Ealet, M. H. Elyakhloufi, E. Gillet and M. Ricci

Laboratoire de Microscopie et Diffractions Electroniques-SERMEC, Case 261, Faculté des Sciences et Techniques de St Jérôme, F-13397 Marseille Cedex 20, France

(Received October 28, 1993; accepted March 16, 1994)

Abstract

We have investigated the crystallographic and electronic structure of γ-alumina surfaces obtained by thermal oxidation of Al foil. By combining X-ray photoelectron spectroscopy, electron energy loss spectroscopy, transmission electron microscopy and transmission electron diffraction investigations, we have shown that such γ-alumina surfaces are mainly (100), (1$\bar{1}$0) and (112) oriented and are characterized by a specific electronic structure in the band gap. The appearance of defect levels decreases the gap from 8.7 eV to 2.5 eV at the surface. These features are correlated to the ionicity of the γ-alumina surface and could explain their chemical activity (*i.e.* acido-basic properties).

1. Introduction

The properties of alumina materials present a great interest in various application areas such as catalysis, coatings, microelectronics, and composite and advanced material technology. In our group, studies have been carried out for some years on the growth and characterization of metal-oxide used for experiments in catalysis [1–3] and thin film adhesion [4–6]. The samples were prepared by metal deposition on alumina surfaces under ultrahigh vacuum (UHV). Several complementary methods were used: secondary ion mass spectrometry (SIMS), transmission electron microscopy (TEM), transmission electron diffraction (TED), Auger electron spectroscopy (AES), electron energy loss spectroscopy (EELS) and X-ray photoelectron spectroscopy (XPS) with the view of determining the electronic structure of the metal–oxide interface in relation to the crystallographic structure. The part of the surface support during the first stages of the growth process has been evidenced and it appeared that the characterization of the interface must be supported by the knowledge of the physical and chemical state of the surface substrate. Well-defined surfaces can be obtained on sapphire single crystals [7]. Nevertheless these samples do not permit easily TEM analysis and it was necessary to prepare thin alumina films as a support for metal deposits. For the most part, the elaboration mode of such samples leads to transition alumina, particularly to γ-alumina which is used in heterogeneous catalysis. Their surfaces contain chemical defects created by dehydroxylation which act catalytically or as potential binding sites of active species [8]. The activity of alumina surfaces can be analyzed in terms of acid–base interactions in the Lewis definition [8, 9], *i.e.* the surface ability for electronic exchanges with other species which can be determined by XPS and related to the variation of the electronic structure [10, 11]. Some studies have been focused on the electronic structure of γ-alumina thin films [12, 13], they have evidenced only few changes in the electronic structure between α and γ alumina. The crystallographic structure of γ-alumina has yet to be determined [14, 15]. Nevertheless all these works concerned the bulk material, and there is a lack of knowledge of the properties of the two or three first layers which are determinant in catalysis or in metal deposit growth.

2. Experimental details

2.1. Sample preparation

Several methods have been tried in our group with the object of obtaining alumina thin films: reactive sputtering, anodic oxidation, and electron bombardment of alumina powder. These processes have given rise to deposits which appear carbon contaminated and non-stoichiometric in AES analysis. Furthermore, electron diffraction analyses have proved that most of the samples are amorphous or constitute a mixture of various alumina phases (γ, η, θ). According to the oxidation methods described in the literature [13, 16–20], a preparation process by thermal oxidation in air of an aluminum foil has been set in the laboratory [21]. Polycrystalline aluminum foils (99.99% purity, Goodfellow Ltd., Mg, 1.2 ppm; Si. 0.8 ppm; Fe. 0.3 ppm; Cu, 0.3 ppm) were used. They are cleaned in a 10% NaOH water solution, rinsed in pure water before to be heated

0040-6090/94/$7.00
SSDI 0040-6090(94)06139-C

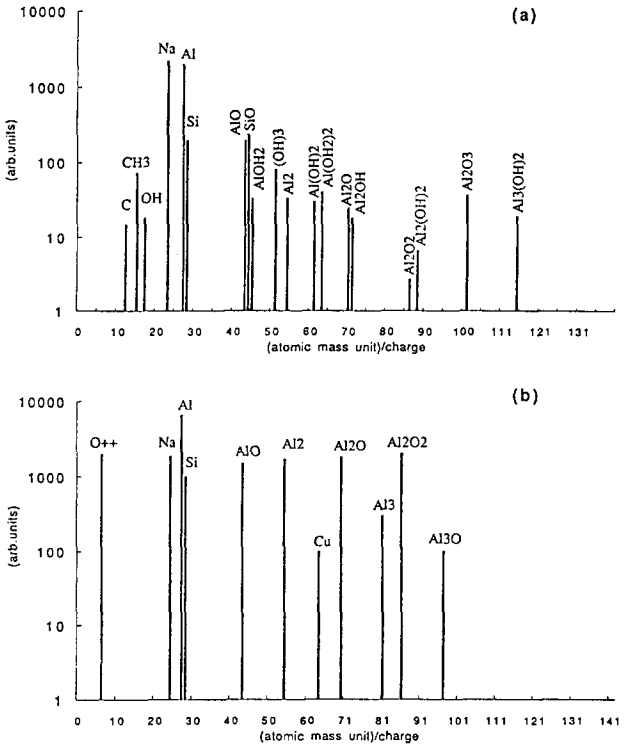

Fig. 1. SIMS patterns obtained on γ-alumina surfaces illustrating the cleaning process. (a) Oxidized aluminum just after cooling. In addition to expected ions (Al^+, AlO^+, Al_2O^+), ions owing to fragmentation of $Al_m(OH)_n$ hydroxyl group and contamination (Na, Si, C) are present. (b) After treatment (argon ion bombardment and annealing at 673 K). The surface is regarded as clean.

at 873 K for 24 h and cooled in air. The alumina surfaces prepared by this method still contain a low contamination level which can be easily removed before use. A SIMS pattern characteristic of such alumina surfaces just after cooling (Fig. 1(a)) points out in addition to the expected species (Al^+, AlO^+, Al_2O^+), some ions owing to the fragmentation of $Al_m(OH)_n$ hydroxyl group. A cleaning process has been set by checking the surface by SIMS before and after treatment. The sample is first submitted to argon ion bombardment (1 kV, 10^{-8} A cm^{-2}) which removes adventitious C, Na, K. After heating at 673 K in UHV for 2 h, the sample is considered clean (Fig. 1(b)). It is possible to state that the hydroxylation of alumina concerns only the first layers of the sample since the shape of the O 1s peak (see Section 5) obtained by XPS analysis reveals only one chemical state.

2.2. Characterization process

After cooling in air, the sample is either prepared for TEM analysis or introduced in the UHV chamber and submitted to the cleaning procedure before EELS or XPS analysis. In a previous work, we have shown [7] that these two complementary methods allow the electronic structure of the alumina surfaces to be determined. Indeed, if some energy-loss features are assigned to plasmon losses, the others can be interpreted as interband transitions with a model of one electron. The interband transition is an electronic excitation from bound state (valence or core) to an unoccupied state located in the conduction band or in the band gap. The XPS data provide us with the energy positions of the initial states. The energy of the final state is determined by adding the energy of the loss (owing to interband transition) to an initial energy state value. For each final-empty-state energy, we take the average of the calculated energy value. Thus, the transition energy agrees with the energy-loss value with an accuracy of 0.3 eV.

EELS measurements were performed in a UHV chamber equipped with a cylindrical mirror analyser (Riber, 10 kV coaxial gun) under normal incidence in the first derivative mode using a primary energy of 100 eV and a modulation amplitude of 1 eV peak to peak. Under these conditions the resolution is better than 0.5 eV.

For XPS analysis, we used a second UHV chamber equipped with a dual Al/Mg X-ray source and a hemispherical analyzer (HA 100 VSW Scientific Instruments). In the present work, the Al Kα line (1486.6 eV) was used; the spectrometer was calibrated using silver and gold samples (Au $4f_{7/2}$ (368.0 eV), Ag $3d_{5/2}$(83.8 eV)). The full width at half maximum (FWHM) of these two peaks is 2.0 eV and 2.2 eV respectively. Alumina surfaces are characterized by the Al 2p, Al 2s, O 2s, and O 1s lines, the valence band and the Al ($KL_{23}L_{23}$), O ($KL_{23}L_{23}$) Auger transitions. During the measurements the pressure in the chamber remained below 1.4×10^{-6} Pa.

The main problem in XPS analysis on insulating samples is the calibration of the kinetic energy scale. The Fermi level is not defined, furthermore charging effects sometimes shift the energy positions of the peaks. Absolute values of the energy levels are difficult to measure, thus all the binding and kinetic energies were referenced to the 1s level of adventitious atoms of C (BE = 284.5 eV). Binding energies were measured with a precision of 0.1 eV.

3. TEM and TED measurements

Oxidized aluminum foils are made of one pure aluminum film sandwiched between two alumina layers which have been found 7.5–10 nm thick (see Section 5.4). Alumina samples are detached by dissolution in a NaOH solution, rinsed in pure water and cut into small pieces to be mounted on grids for TEM and TED observations. A characteristic TEM image obtained with such samples is shown in Fig. 2. Alumina foils are

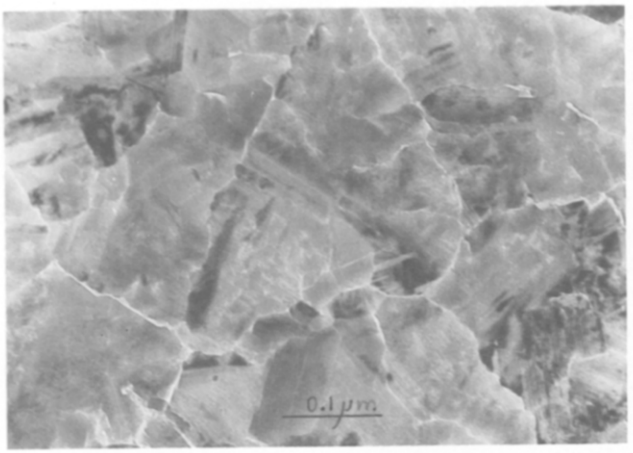

Fig. 2. TEM micrograph of a γ-alumina layer (electron primary energy, $E_p = 100$ keV). The mean grain size occurs in the 0.1–0.5 mm range.

polycrystalline, the mean grain size occurring in the 0.1–0.5 mm range. Therefore they are well suited for selected area diffraction. The more often observed TED patterns are presented in Figs. 3(a)–3(c) together with the indexed schematic diagrams. The reflections are sharp without extra lines and the indices given in Figs. 3(a)–3(c) indicate a perfect γ-alumina lattice (spinel structure) without disorder in the cubic-close-packing [14]. Lippens and De Boer [15] have shown that a disorder in the tetrahedral sites occupation can exist. In this case, two new reflections appear in the diffraction patterns, (002) and (006). The diffraction patterns of the oxidized films that we prepare do not show such reflections. Thus it can be expected that aluminum atoms are set regularly in tetrahedral sites. The patterns of Fig. 3 have been interpreted by (100), (1$\bar{1}$0) and (112) orientations with appearence percentages of 80%,

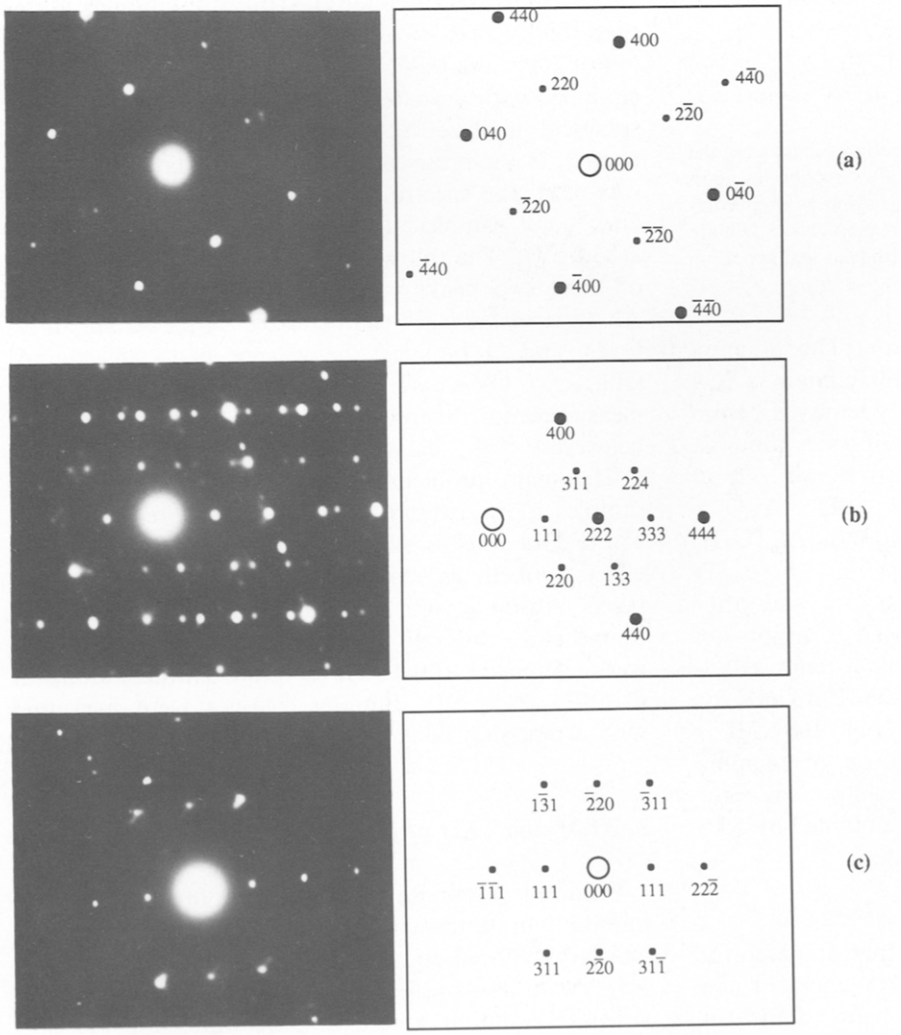

Fig. 3. Diffraction patterns obtained by selected area diffraction on the crystallites of γ-alumina ($E_p = 100$ keV). Only the more frequent patterns are presented in (a), (b) and (c). They correspond respectively to (100), (1$\bar{1}$0) and (112) orientations in a spinel structure. The indices of reflections are reported on the adjacent drawings. Extra spots observed in the (1$\bar{1}$0) pattern are given by a twinning along the (111) planes.

10%, 10% respectively. Extra spots are sometimes observed (Fig. 3(b)) and they can easily be interpreted by twinning along the (111) plane [22]. It is noteworthy that twins have only been observed in the (1$\bar{1}$0) oriented crystals.

4. Crystallographic structure

4.1. Bulk structure

The alumina structure depends largely on the hydroxylation state. After baking in UHV the γ-alumina do not contain hydroxyl groups. They have a crystal lattice close to that of the $MgAl_2O_4$ spinel structure.

The unit cell of $MgAl_2O_4$ is formed by 32 atoms of oxygen which form a cubic-close-packing arrangement, 16 atoms of aluminum in octahedral interstices and 8 atoms of magnesium in tetrahedral sites. The γ-alumina differ from this lattice by the number of Al atoms in the interstices. The unit cell contains $21^{1/3}$ aluminum atoms which are divided onto octahedral and tetrahedral positions creating $2^{2/3}$ vacancies. The proportion of occupation of octahedral and tetrahedral positions is 2:1. TED analysis has shown that cation vacancies are not randomly distributed, so we have proposed a lattice model deduced from the α-alumina unit mesh [23]. The cubic-close-packing unit cell is formed by 12 compact layers with the packing sequence AB AB AB ... (Fig. 4). In these planes the aluminum atoms are located in octahedral positions and in the vacancies. The aluminum atoms in tetrahedral positions, located between the A and B planes, are divided into three planes labelled C, D, E. The whole γ-Al_2O_3 mesh is obtained by the sequence ACBD ACBE ACBD ACBE ACBD ACBE.

4.2. Atomic models of the surface samples

The TED and TEM measurements have shown that alumina layers are polycrystalline. However, the grains are mainly (100) oriented: (1$\bar{1}$0) and (112) orientations being less prevalent.

The (100) surface has an Al_2O_4 stoichiometry. The aluminum atoms, located in octahedral sites, are five-fold coordinated: they are linked to four oxygen atoms of the first layer and one oxygen of the second layer (Fig. 5(a)). The (1$\bar{1}$0) and (112) planes can give either pure oxygen surfaces or mixed Al, O surfaces; they

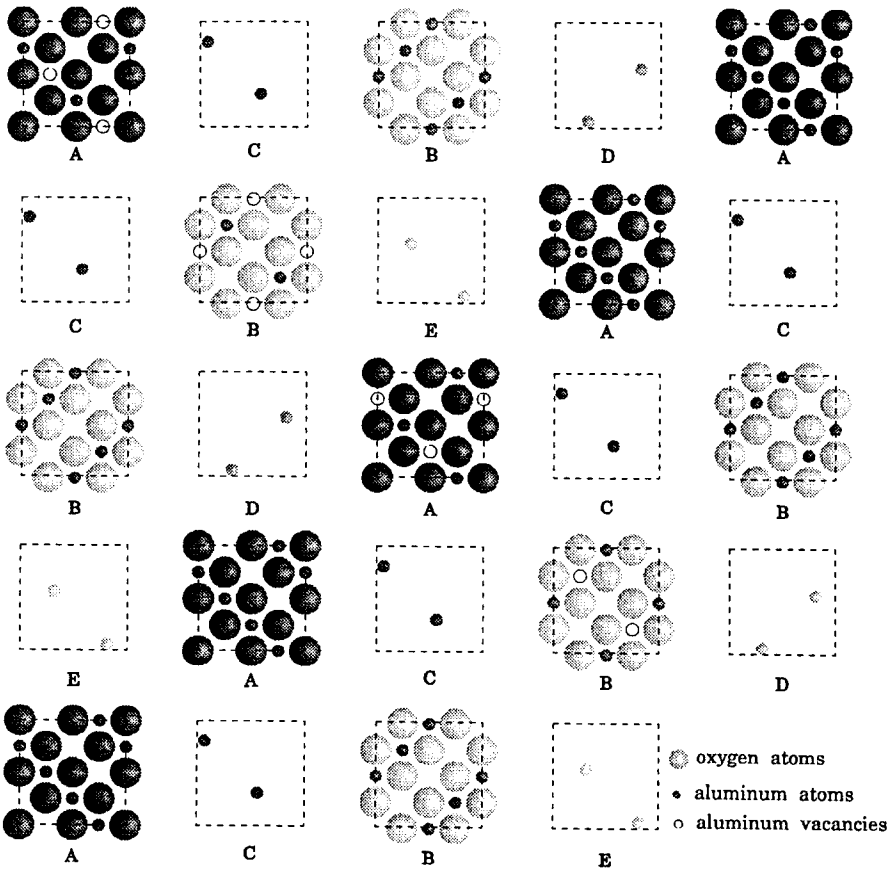

Fig. 4. Successive layers ACBD ACBE ACBD ACBE ACBD ACBE which constitute the γ-Al_2O_3 unit cell. In the planes A and B, the aluminum atoms are in octahedral sites. The planes C, D, E are constituted by aluminum atoms in tetrahedral coordination. The aluminum vacancies are set in octahedral sites.

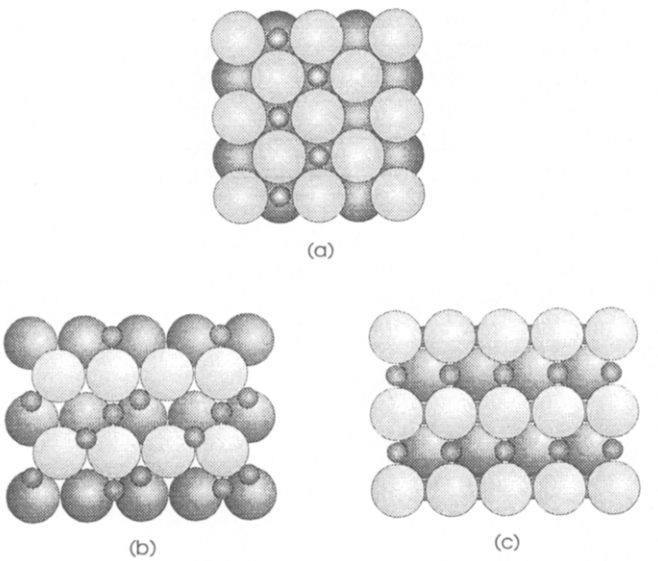

Fig. 5. Examples of planes obtained by cutting the bulk of the γ-alumina network: (a) (100) plane, (b) and (c) (1$\bar{1}$0) plane. They illustrate the existence of various surface stoichiometries (AlO, Al_3O_4, Al_5O_4). (c) presents the possibility of a plane made up only of oxygen atoms.

differ by the number of aluminum cations in octahedral positions. The aluminum atoms in octahedral positions are four-fold coordinated whereas the coordination number of atoms in the tetrahedral positions is three. These surfaces exhibit different stoichiometries: AlO, Al_3O_4, Al_5O_4. As an example, we present four models of the (1$\bar{1}$0) surface (Figs. 5(b)–5(c)).

It is therefore possible to state that most of the surfaces have a stoichiometry lower than the bulk and would give rise to different behaviour with respect to admolecules or adatoms.

5. XPS and EELS measurements

5.1. Alumina film thickness

The XPS studies were performed on alumina layers supported on aluminum foil. It has been shown that the binding energy shift of Al 2p lines varies in the 2.6–3.7 eV range depending on the oxide thickness [18]. The Al 2p peak obtained for a thickness lower than 7.5 nm can be fitted by the sum of a gaussian peak which represents the oxide component, and a non-gaussian peak which is characteristic of the metallic component. Comparison of the intensity of the two peaks allows the determination of the oxide thickness.

In the present work, aluminum has been detected in only one chemical state. The position and the shape of the Al 2p peak corresponds to γ-alumina (Fig. 6(a)). Therefore, following the Seah's empirical analysis [24], the thickness of the oxide would be three times the

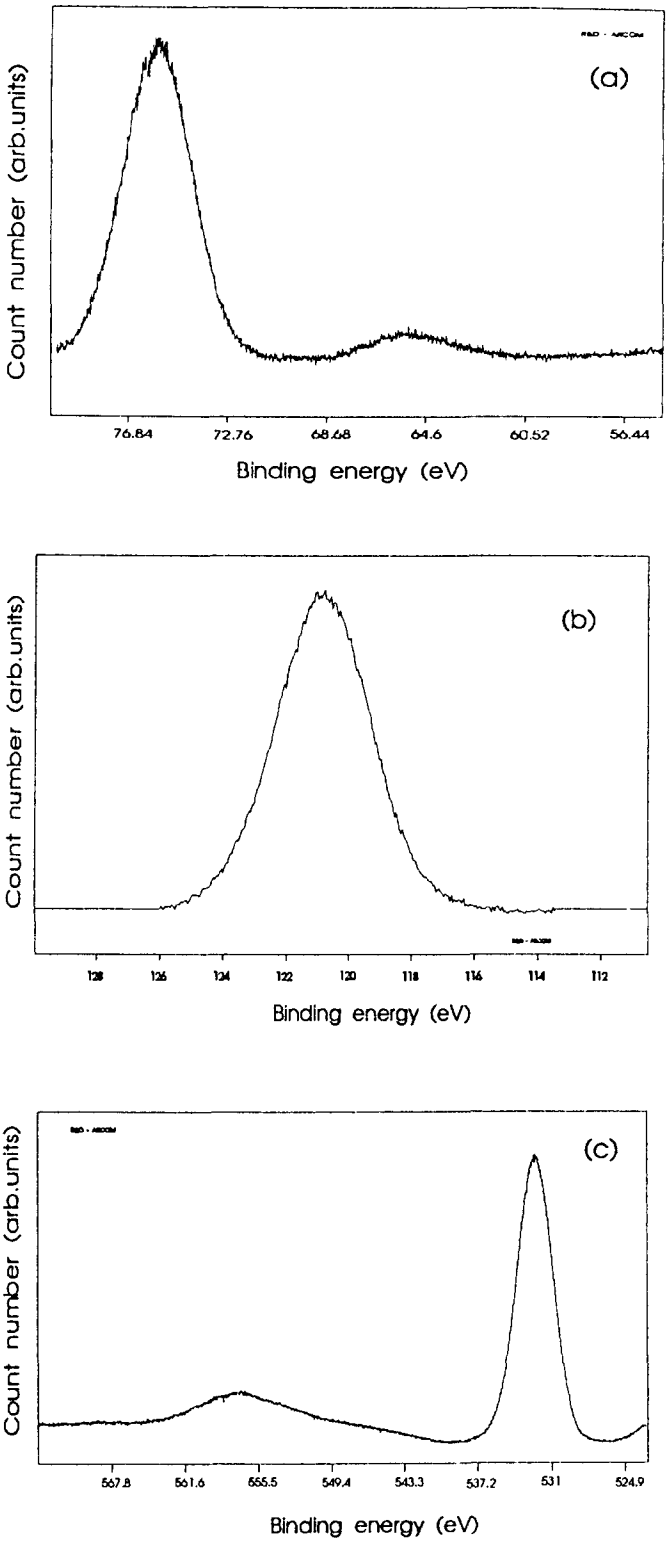

Fig. 6. X-ray photoelectron spectra of 2p (a) and 2s (b) core levels of aluminum and the 1s core level of oxygen (c) obtained on γ-alumina. The position and the shape of the Al 2p peak correspond with only one chemical state for an aluminum species and indicate an oxide thickness larger than 7.5 nm. The O 1s peak exhibits a gaussian shape which indicates only one chemical state for oxygen. The O 1s satellite on the high energy side corresponds with the bulk plasmon.

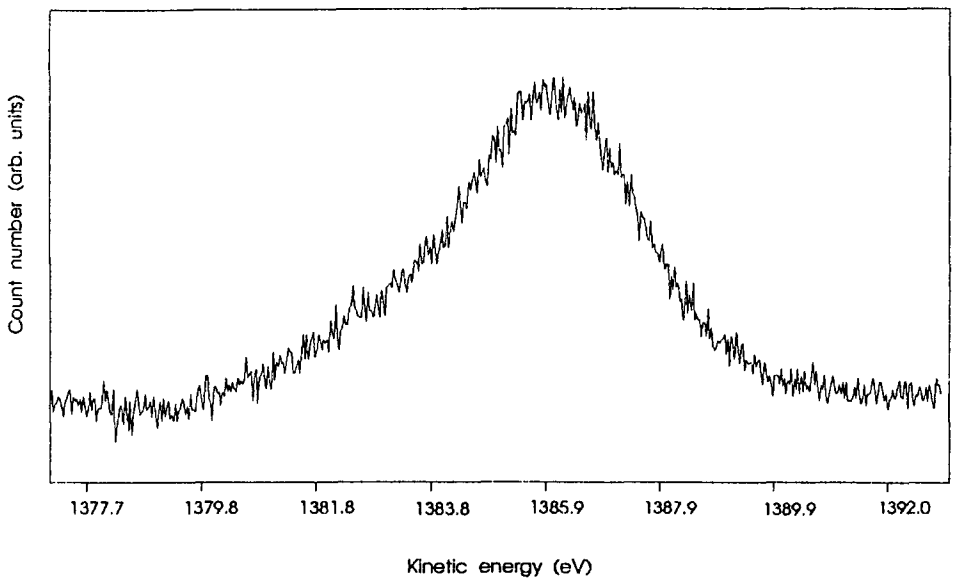

Fig. 7. Spectrum of the Al ($KL_{23}L_{23}$) Auger transition obtained by XPS. The peak occurs at a kinetic energy of 1385.9 eV which is characteristic of the Al^{3+} species.

inelastic mean free path of the photoelectron in the oxide. In another study the thickness of the oxide obtained by a similar process has been found around 40 nm [20], consequently, we estimated the thickness of alumina layers in the 7.5–40 nm range.

5.2. Electronic structure

Figures 6(a)–6(c) show the Al 2p, Al 2s and O 1s photoelectron emission which occur at kinetic energies of 1411.0, 1365.7 and 953.8 eV respectively, *i.e.* at binding energies of 75.6, 120.9 and 532.8 eV. These values are in good agreement with earlier studies [12, 13, 25]. The O 1s peak exhibits a gaussian shape which indicates only one chemical state for oxygen atoms at the surface [26].

The Al ($KL_{23}L_{23}$) Auger line is presented in Fig. 7. The kinetic energy of the Auger peak for metallic aluminum (Al^0 1392.0 eV) is shifted of 6 eV above the kinetic energy of Al^{3+} [12]. We observe only one chemical state for the aluminum species at kinetic energy of 1385.9 eV.

The main peak of the O (KLL) Auger series: O ($KL_{23}L_{23}$), occurs at a kinetic energy of 505.8 eV (Fig. 8). The shoulder on the high kinetic energy side

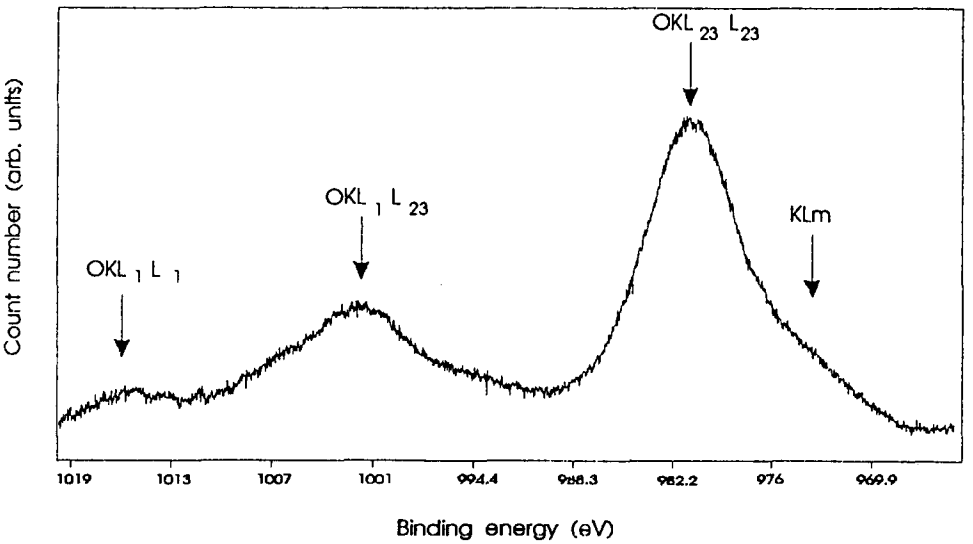

Fig. 8. Spectrum of O (KLL) Auger lines. The three transitions KL_1L_1, KL_1L_{23} and $KL_{23}L_{23}$ are visible. The shoulder (KL_m) on the high energy side of the $KL_{23}L_{23}$ transition corresponds to a transition from KL oxygen level to an aluminium level labelled *m*.

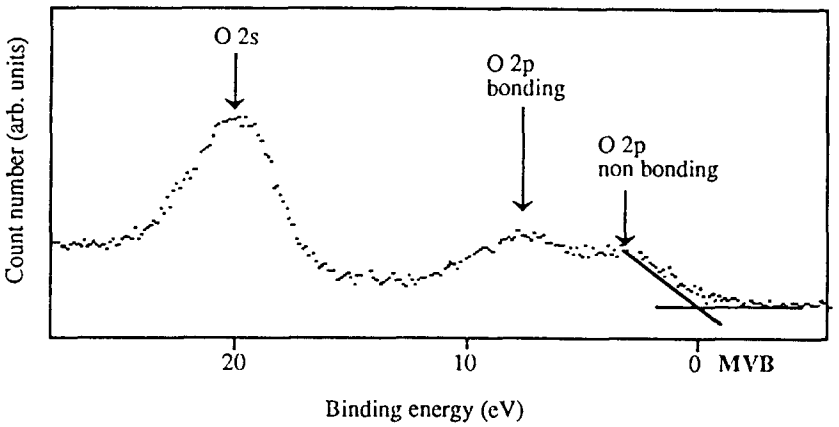

Fig. 9. Valence band of γ-alumina obtained by XPS. The valence band is divided into two parts: the UVB with two maxima O 2p bonding and O 2p non-bonding orbitals, and the LVB constituting O 2s orbitals. The UVB is mainly created by O 2p bonding and non-bonding orbitals with a small component of Al 3s and Al 3p orbitals.

has been interpreted as a KL-*m* interatomic transition: a transition from the KL level of oxygen to an aluminum level labelled *m* [12].

The valence band region (Fig. 9) can be divided into two parts: the upper valence band (UVB) in the 0–10 eV energy range and the lower valence band (LVB) in the 15–21 eV energy range. In Fig. 9 the energies are referenced to the valence band maximum (VBM). The UVB is mainly created by O 2p bonding and non-bonding orbitals with a small component of Al 3s and Al 3p orbitals [27]. In Fig. 9, we observe two maxima labelled O 2p non-bonding and O 2p bonding in spite of the contribution of Al orbitals. The UVB width is of 9.5 eV. The LVB is constituted by O 2s orbitals with a maximum located at 20.3 eV below VBM.

The shape of the valence band can be correlated with the Al^{3+} ions distribution in octahedral and tetrahedral sites. The relative height of the two maxima of the valence band varies following the coordination of the aluminum atoms in the oxygen lattice [9]. We always observed that the intensities of the two peaks are quite the same illustrating an occupation of the two kinds of sites.

By using the values of Al 2p binding energy and Al ($KL_{23}L_{23}$) kinetic energy, we calculate the Auger parameter as defined by Wagner *et al.* [28]. The Auger parameter is a good tool to determine the phase, the stoichiometry and the crystallinity of alumina surfaces [12, 29]. Indeed the Auger parameters of α- and γ-alumina are 1462.0 eV and 1461.4 eV respectively [29]. Our measurements lead to a value of 1461.6 eV which is in good agreement with previous results.

An energy loss spectrum obtained on γ-alumina is presented in Fig. 10(a). By the method described in Section 2.2, we obtain the transition diagram shown in Fig. 10(b) which justifies the loss values. Only the transitions involving maximum densities of state in the conduction band have been considered. In the diagram, the energies of the levels, referenced to the conduction band minimum (CB_{min}), are shifted 8.7 eV (value of the gap E_g) with regard to the VBM.

For energy loss values lower than E_g, the final state takes place in the band gap. It has already been shown that the final states in the gap are introduced by defects [30, 31]. The γ-alumina surface is characterized by its own gap structure (Fig. 10(b)) with empty levels at 3.9, 5.3 and 6.2 eV below CB_{min}. The level at 5.3 eV below the CB_{min} is an intrinsic level characteristic of the creation of the surface. Such a level has been found theoretically or experimentally on α-alumina [8, 29]. The level at 3.9 eV below CB_{min} is created by dangling Al spz bonds at the surface. The level at 6.2 eV below CB_{min} can be interpreted by comparison with the electronic structure of α-alumina [7] as an enlargement of the 5.3 eV level. It appears when the oxide stoichiometry decreases.

The decrease of the band gap induces a shift in the position of the Fermi level which can be correlated with the ability of the surface to give or accept electrons [10, 11]. It has been shown that a decrease (increase) of the Fermi energy (*i.e.* $E_F - E_{VBM}$) introduces an increase in the donor (acceptor) behaviour. On γ-alumina surfaces, the decrease of the band gap has been interpreted as an increase in the basic behaviour at the surface which will have some important effects on the surface chemistry [11, 32].

The appearance of levels in the band gap decreases the gap from 8.7 eV for the bulk to 2.5 eV for the surface, then such a surface cannot be considered as insulating but as a new phase with different properties which has been characterized by the decrease of the ionicity of oxygen sites. Indeed, the charge of the oxygen atoms depends in a large part on the chemical bond between the oxygen atom and its neighbours. The

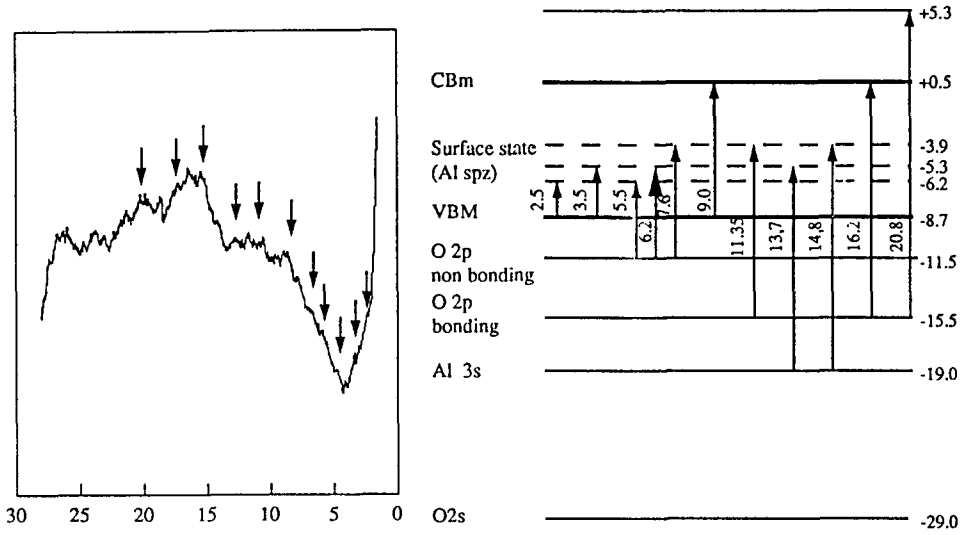

(a) (b)

Fig. 10. Electronic structure of γ-alumina obtained by EELS. The spectrum of energy loss (a) is realised with a primary energy of 100 eV. The transition diagram (b) is calculated in the one electron model for direct interband transitions.

study of the Auger transitions of oxygen allows the determination of the ionicity of the oxygen sites by measuring of the height and the energetic position of the two larger oxygen transitions: $KL_{23}L_{23}$ and KL_1L_{23}. Ascarelli and Moretti [33] have shown that the ionicity of the oxygen sites increases when the ratio $f(I_{KL23L23}: I_{KL1L23})$ of the intensity decreases while the energy difference $E_{KL23L23} - E_{KL1L23}$ increases. In order to characterize the variation of the charge for different alumina surfaces, monocrystalline, polycrystalline, alpha, gamma, stoichiometric or oxygen deficient (called reduced), we have plotted the ratio of the Auger line intensity as a function of $E_{KL23L23} - E_{KL1L23}$ (Fig. 11). The results indicate that the ionicity decreases through

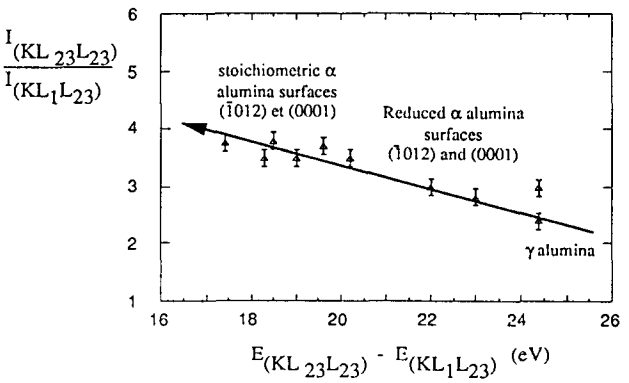

Fig. 11. Evolution of the ionicity for different alumina surfaces: γ, α, reduced α-alumina and stoichiometric α-alumina. The arrow indicates the increase of the ionicity following ref. 32.

the series stoichiometric α-alumina, reduced α-alumina, γ-alumina layers, which is in accordance with the observations reported in ref. 28.

6. Conclusion

In this work, we have presented a crystallographic and spectroscopic study of γ-alumina thin films obtained by thermal oxidation of aluminum foils. This preparation process leads to the formation of polycrystalline films with three main orientations: (100), (1$\bar{1}$0) and (112). The crystallographic analysis of these surfaces suggests that the stoichiometry of the oxide layer surface is lower than the stoichiometry of the bulk. This result is supported by the XPS and AES measurements. We state that the reduction of the stoichiometry induces the appearance of defect levels located in the band gap which decreases the band gap from 8.7 eV to 2.5 eV at the surface. Similar results have been found on reduced α-alumina surfaces [7]. Such a general behaviour suggests the existence on the oxide surface of a material different from the bulk which cannot be considered as insulating. The comparison of γ-alumina with α-alumina shows a decrease of the ionicity through the series stoichiometric α-alumina, reduced α-alumina, γ-alumina layers. These results are to be taken into account to explain the acido-basic properties of technological alumina powders used as catalysts or as support for metal particles in heterogeneous catalysis.

References

1 F. Robinson and M. Gillet, *Thin Solid Films*, *98* (1982) 179.
2 A. Renou, *Thèse de doctorat d'Etat*, Marseille, 1979.
3 T. Lahouari, *Thèse de 3ème cycle*, Université Aix Marseille III, 1987.
4 V. Matolín and E. Gillet , *Vacuum*, *36* (1986) 449.
5 N. Kruse and E. Gillet, *Z. Phys. D*, *12* (1989) 575.
6 V. Matolín, E. Gillet, N.M. Reed and J.C. Vickerman, *J. Chem. Soc. Faraday Trans.*, *86* (1990) 2749.
7 E. Gillet and B. Ealet, *Surf. Sci.*, *273* (1992) 427.
8 D. L. Cocke, E. D. Johnson and R. P. Merrill, *Catal. Rev. Sci. Eng.*, *26* (1984) 163.
9 F. W. Fowkes, *J. Adhes. Sci. Technol.*, *1* (1987) 7.
10 M. Casamassima, E. Darque-Ceretti, A. Etcheberry and M. Aucoutinier, *Appl. Surf. Sci.*, *52* (1991) 205.
11 W. M. Mullins and B. L. Averbach, *Surf. Sci.*, *206* (1988) 52.
12 B. G. Frederick, G. Apai and T. N. Rhodin, *Surf. Sci.*, *244* (1991) 67.
13 A. Jimenéz-Gonzaléz and D. Scheisser, *Surf. Sci.*, *250* (1991) 59.
14 B. C. Lippens and J. J. Steggenda, *Physical and Chemical Aspects of Adsorbants and Catalysts*, Science Press, London, 1970.
15 B. C. Lippens and J. H. De Boer, *Acta Crystallogr.*, *17* (1964) 1312.
16 I. P. Batra and L. Kleinman, *J. Electron Spectrosc. Relat. Phenom.*, *33* (1984) 175.
17 H. J. Mathieu, M. Datta and D. Landolt, *J. Vac. Sci. Technol. A*, *3* (1985) 331.
18 R. L. Tapping, R. D. Davidson, T. E. Jackman and J. A. Davies, *Surf. Interf. Anal.*, *11* (1988) 441.
19 P. V. Thomas, V. Ramakrishnan and V. K. Vaidyan, *Thin Solid Films*, *170* (1989) 35.
20 H. J. Van Beek and E.J. Mittemeijer, *Thin Solid Films*, *122* (1984) 131.
21 M. Ricci, *Thèse*, Université Aix-Marseille III, 1991.
22 Z. G. Pinsker, *Electron Diffraction*, Butterworths Scientific Publications, 1953, p. 234.
23 B. Ealet, *Thesis*, Université Aix-Marseille III, 1993.
24 M. P. Seah and W. A. Dench, *Surf. Interf. Anal.*, *1* (1979) 2.
25 A. Balzarotti and A. Bianconi, *Phys. Stat. Sol. (b)*, *76* (1976) 689.
26 B. R. Strohmeier, *Surf. Interf. Anal.*, *15* (1990) 51.
27 M. Kefi, P. Jonnard, F. Vergand, C. Bonnelle and E. Gillet, *J. Phys. Conden. Matter*, *5* (1993) 8629.
28 C. D. Wagner, L. H. Gale and R. H. Raymond, *Anal. Chem.*, *51* (1979) 466.
29 C. D. Wagner, D. E. Passoja, H. J. Hillery, T. G. Kinisky, H. A. Six, W. T. Jansen and J. A. Taylor, *J. Vac. Sci. Technol.*, *21* (1982) 933.
30 W. J. Gignac, R. S. Williams and S. P. Kowalczyk, *Phys. Rev. B*, *32* (1985) 1237.
31 S. Ciraci and I. P. Batra, *Phys. Rev. B*, *28* (1983) 982.
32 W. M. Mullins, *Surf. Sci.*, *217* (1989) 459.
33 P. Ascarelli and G. Moretti, *Surf. Interf. Anal.*, *7* (1985) 8.